

# Adaptive boundary conditions for exterior flow problems

Sebastian Bönisch\*

Numerical Analysis group, IWR

University of Heidelberg

sebastian.boenisch@iwr.uni-heidelberg.de

Vincent Heuveline\*

Numerical Analysis group, IWR

University of Heidelberg

vincent.heuveline@iwr.uni-heidelberg.de

Peter Wittwer†

Département de Physique Théorique

Université de Genève, Switzerland

peter.wittwer@physics.unige.ch

April 16, 2003

## Abstract

We consider the problem of solving numerically the stationary incompressible Navier-Stokes equations in an exterior domain in two dimensions. This corresponds to studying the stationary fluid flow past a body. The necessity to truncate for numerical purposes the infinite exterior domain to a finite domain leads to the problem of finding appropriate boundary conditions on the surface of the truncated domain. We solve this problem by providing a vector field describing the leading asymptotic behavior of the solution. This vector field is given in the form of an explicit expression depending on a real parameter. We show that this parameter can be determined from the total drag exerted on the body. Using this fact we set up a self-consistent numerical scheme that determines the parameter, and hence the boundary conditions and the drag, as part of the solution process. We compare the values of the drag obtained with our adaptive scheme with the results from using traditional constant boundary conditions. Computational times are typically reduced by several orders of magnitude.

## 1 Introduction

Consider a rigid body that is placed into a uniform stream of a homogeneous incompressible fluid, filling all of  $\mathbf{R}^2$ . This situation is modeled by the Navier-Stokes equations

$$\begin{aligned} -\rho(\mathbf{u} \cdot \nabla)\mathbf{u} + \mu\Delta\mathbf{u} - \nabla p &= 0, \\ \nabla \cdot \mathbf{u} &= 0, \end{aligned} \tag{1}$$

in  $\Omega = \mathbf{R}^2 \setminus \mathbf{B}$ , with  $\mathbf{B}$  a compact domain (the body), subject to the boundary conditions  $\mathbf{u}|_{\partial\mathbf{B}} = 0$  and  $\lim_{|\mathbf{x}| \rightarrow \infty} \mathbf{u}(\mathbf{x}) = \mathbf{v}_\infty$ . Here,  $\mathbf{u}$  is the velocity field,  $p$  is the pressure and  $\mathbf{v}_\infty$  is some constant non-zero vector field which we choose without restriction of generality to be parallel to the  $x$ -axis, i.e.,  $\mathbf{v}_\infty = (v_\infty, 0)$  and  $v_\infty > 0$ . The density  $\rho$  and the dynamic viscosity  $\mu$  are arbitrary positive constants. For simplicity, we restrict ourselves here to domains and flows that are symmetric with respect to the  $x$ -axis. The asymmetric case (case with lift) is more complicated and will be treated elsewhere.

When solving problem (1) numerically one is confronted with the necessity to truncate the exterior infinite domain  $\Omega$  to a finite domain  $D \subset \Omega$  (see Figure 1). This means, however, that appropriate boundary conditions have to be found on the surface  $\Gamma = \partial D \setminus \partial\mathbf{B}$  of the truncated domain. The problem of choosing these so called artificial boundary conditions has only recently been treated in the mathematics literature (see for example [19]), but has not led to explicit enough prescriptions to be used in numerical work.

---

\*Supported by the SFB 359 “Reaktive Strömungen, Diffusion und Transport” and the BMBF (Bundesministerium für Bildung und Forschung) project under grant 03.RAM.3HD

†Supported in part by the Fonds National Suisse de la Recherche Scientifique.

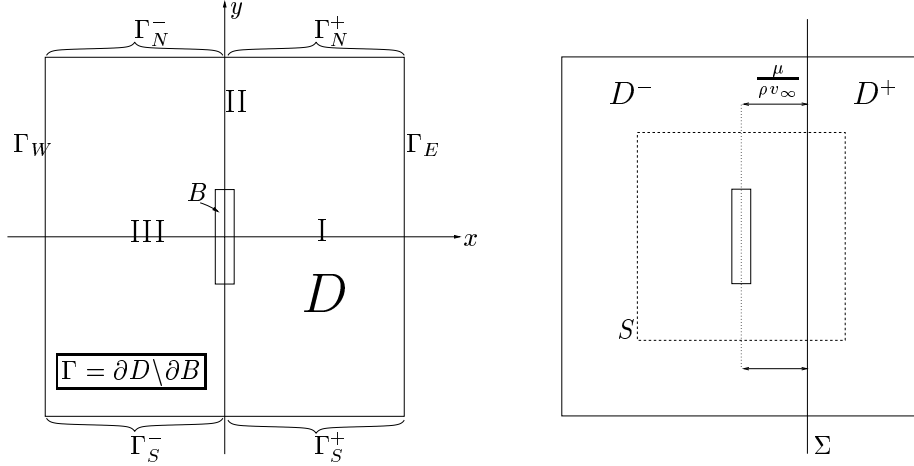


Figure 1: Description and notations of the considered exterior flow problem.

Here, using the recent results in [28], [29] we construct an explicit vector field which we use on the boundary of the truncated domain. This idea is related to results in [9], for example, where it is shown that the solution of the nonlinear problem (1) is at large distances asymptotic to a solution of the corresponding linearized problem, the Oseen problem, and in [19] it is shown that the use of this solution a priori provides a good way of prescribing artificial boundary conditions. However, since the solution of the linear problem is only unique up to some unknown multiplicative constant, this idea has not been put into practice numerically. Our solution to this problem uses a “fact” that is well known in the engineering literature [4]. Namely, we show that the unknown multiplicative constant is in appropriate units equal to the total drag exerted on the body and can therefore be computed along with the vector field using a self-consistency condition between the imposed boundary condition and the resulting drag. It is this idea that is put into practice below.

In order to solve equation (1) numerically, it is more convenient to set  $\mathbf{u} = \mathbf{v}_\infty + \mathbf{v}$ , with

$$\mathbf{v} = (u, v), \quad (2)$$

and to study the equation

$$\begin{aligned} -\rho(\mathbf{v}_\infty \cdot \nabla)\mathbf{v} - \rho(\mathbf{v} \cdot \nabla)\mathbf{v} + \mu\Delta\mathbf{v} - \nabla p &= 0, \\ \nabla \cdot \mathbf{v} &= 0, \end{aligned} \quad (3)$$

with boundary conditions  $\mathbf{v}|_{\partial B} = -\mathbf{v}_\infty$  and  $\lim_{|\mathbf{x}| \rightarrow \infty} \mathbf{v}(\mathbf{x}) = 0$ .

Note that, in contrast to the finite volume case, the boundary conditions do not prescribe the total flux of fluid (from left to right say). In particular, it does not follow from  $\lim_{|\mathbf{x}| \rightarrow \infty} \mathbf{v}(\mathbf{x}) = 0$  that  $\int_{-\infty}^{\infty} u(x, y) dy = 0$ , the correct and non-zero value of these integrals<sup>1</sup> being intimately related to the total force exerted on the body (see below).

As mentioned above it is this fact which makes the numerical implementation of (3) challenging, since the prescription of a vector field on the boundary  $\Gamma$  also fixes the total flux across the finite domain  $D$ . It is therefore in a way quite astonishing that the solutions of (3) converge, for an increasing sequence of domains  $D$  with Dirichlet boundary conditions on  $\Gamma$ , to the solution of the infinite volume problem [18]. This convergence is however very slow, since an artificial backflow (of small amplitude) has to be created on a big portion of the domain  $D$  in order to accommodate for the zero flux condition enforced by Dirichlet boundary conditions (see upper half of Figure 2). With our adaptive boundary conditions the flux through  $D$  is “exactly right”, and no portion of the volume  $D$  is lost for the computation of a non-physical backflow: the fluid is transported within the wake towards the body, and this fluid is then

<sup>1</sup>From  $\nabla \cdot \mathbf{v} = 0$  and the boundary condition  $\lim_{|\mathbf{x}| \rightarrow \infty} \mathbf{v}(\mathbf{x}) = 0$  it follows using Gauss’ theorem that the limit  $\lim_{L \rightarrow \infty} \int_{-L}^L [u(x_2, y) - u(x_1, y)] dy$  exists and equals zero for arbitrary  $x_1, x_2$ . A stronger result can be found in [29], where it is shown that, under suitable assumptions, the integrals  $\int_{-\infty}^{\infty} u(x, y) dy$ , exist in the  $(C, \delta)$ -sense and are independent of  $x$ .

“radiated” away from the body by a source-like contribution in the velocity field (see lower half of Figure 2).

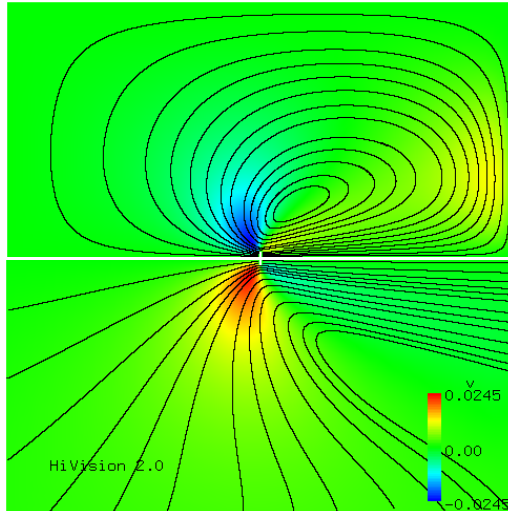


Figure 2: Stream-lines, upper half: the typical nonphysical backflow in the velocity field when imposing homogeneous Dirichlet boundary conditions. Stream-lines, lower half: no backflow is created with adaptive boundary conditions. In the background the component  $v$  of the vector field is shown in order to indicate the size of amplitudes.

The paper is organized as follows. In Section 2 we show how the results from [28], [29] can be used to construct an explicit vector field on the artificial boundary and relate the unknown multiplicative constant to the total drag exerted on the body. In Section 3 we describe the numerical algorithm that has been used to solve (3). In Section 4 we compare the results obtained using the traditional Dirichlet boundary conditions with those obtained from using our adaptive scheme. The difference is impressive: for a given precision the adaptive boundary conditions allow us to take the domain  $D$  approximately ten times smaller, which results in computation times that are more than a factor of hundred shorter. We then use the adaptive boundary conditions to compute the drag for several values of the viscosity, solving in particular also cases which require ridiculously large domains  $D$  when treated using Dirichlet boundary conditions.

## 2 Boundary conditions

Let  $A$  be a “typical” length scale of the domain  $\mathbf{B}$  (its maximal diameter for example). For bodies  $\mathbf{B}$  with smooth boundary  $\partial\mathbf{B}$ , and for small enough Reynolds number

$$Re = \rho v_\infty / \mu , \quad (4)$$

equation (1) is known to have a (strong) solution  $\mathbf{u} = \mathbf{v}_\infty + (u, v)$ ,  $p$ , [9]. If  $\mathbf{B}$  is symmetric with respect to the  $x$ -axis this solution is symmetric, i.e.,  $u$  and  $p$  are even functions of  $y$  for fixed  $x$ , and  $v$  is an odd function of  $y$  for fixed  $x$ . For large Reynolds numbers there is still no complete answer to the existence problem [10]. Solutions still exist in these cases in a weak sense. These solutions can be constructed by considering equation (1) on a nested sequence of finite domains  $D$  with Dirichlet boundary conditions on  $\Gamma$  (see Figure 1) [19]. By choosing a convergent subsequence one obtains a limit that satisfies equation (1) in a weak sense, but not necessarily the boundary condition at infinity.

In Section 4 we will numerically solve (1), (respectively (3)), for a rectangular body on a nested sequence of square domains with Dirichlet boundary conditions. The sequence of these numerical solutions is then compared with solutions obtained via the adaptive boundary conditions that we construct next.

## 2.1 Asymptotic behavior of solution

Let  $\mathbf{u}$ ,  $\mathbf{v}$  and  $p$  be the vector fields and  $p$  the pressure introduced in (1) and (3). We then scale to dimensionless coordinates  $\tilde{\mathbf{x}} = \mathbf{x}/\ell$ , with

$$\ell = \frac{\mu}{v_\infty \rho} \quad (5)$$

the viscous length scale of the problem, and introduce the dimensionless vector fields  $\tilde{\mathbf{u}}$ ,  $\tilde{\mathbf{v}}$  and a dimensionless pressure  $\tilde{p}$  by defining  $\mathbf{u}(\mathbf{x}) = v_\infty \tilde{\mathbf{u}}(\tilde{\mathbf{x}})$  and  $\mathbf{v}(\mathbf{x}) = v_\infty \tilde{\mathbf{v}}(\tilde{\mathbf{x}})$  and  $p(\mathbf{x}) = (\rho v_\infty^2) \tilde{p}(\tilde{\mathbf{x}})$ . Note that  $\tilde{\mathbf{u}} = (1, 0) + \tilde{\mathbf{v}}$ ,  $\tilde{\mathbf{v}} = (\tilde{u}, \tilde{v})$ , and that

$$u(x, y) = v_\infty \tilde{u}(\tilde{x}, \tilde{y}) , \quad (6)$$

$$v(x, y) = v_\infty \tilde{v}(\tilde{x}, \tilde{y}) , \quad (7)$$

with  $(u, v)$  as defined in (2). In dimensionless variables equation (1) becomes

$$\begin{aligned} -(\tilde{\mathbf{u}} \cdot \nabla) \tilde{\mathbf{u}} + \Delta \tilde{\mathbf{u}} - \nabla \tilde{p} &= 0 , \\ \nabla \cdot \tilde{\mathbf{u}} &= 0 , \end{aligned} \quad (8)$$

(derivatives are now taken with respect to the variables  $\tilde{x}$  and  $\tilde{y}$ ). In [28], [29] these equations have been studied in the half-space  $D^+ = \{(\tilde{x}, \tilde{y}) \in \mathbf{R}^2 \mid \tilde{x} \geq 1\}$  (see Figure 1). Under certain smallness assumptions on the vector field  $\tilde{\mathbf{u}}$  on  $\Sigma$  (which we expect in particular to be valid for small enough Reynolds numbers), it has been proved that there are numbers  $c$  and  $d$  and functions  $\tilde{u}_0$ ,  $\tilde{v}_0$ ,

$$\tilde{u}_0(\tilde{x}, \tilde{y}) = \frac{c}{2\sqrt{\pi}} \frac{1}{\sqrt{\tilde{x}}} e^{-\frac{\tilde{y}^2}{4\tilde{x}}} + \frac{d}{\pi} \frac{\tilde{x}}{\tilde{x}^2 + \tilde{y}^2} , \quad (9)$$

$$\tilde{v}_0(\tilde{x}, \tilde{y}) = \frac{c}{4\sqrt{\pi}} \frac{\tilde{y}}{\tilde{x}^{3/2}} e^{-\frac{\tilde{y}^2}{4\tilde{x}}} + \frac{d}{\pi} \frac{\tilde{y}}{\tilde{x}^2 + \tilde{y}^2} , \quad (10)$$

such that

$$\lim_{\tilde{x} \rightarrow \infty} \tilde{x}^{1/2} \left( \sup_{\tilde{y} \in \mathbf{R}} |(\tilde{u} - \tilde{u}_0)(\tilde{x}, \tilde{y})| \right) = 0 , \quad (11)$$

$$\lim_{\tilde{x} \rightarrow \infty} \tilde{x} \left( \sup_{\tilde{y} \in \mathbf{R}} |(\tilde{v} - \tilde{v}_0)(\tilde{x}, \tilde{y})| \right) = 0 . \quad (12)$$

Moreover,

$$\int_{\mathbf{R}} \tilde{u}(\tilde{x}, \tilde{y}) d\tilde{y} = \int_{\mathbf{R}} \tilde{u}_0(\tilde{x}, \tilde{y}) d\tilde{y} = c + d , \quad (13)$$

independently of  $\tilde{x} \geq 1$ . Equations (11) and (12) express the fact that asymptotically, for large values of  $\tilde{x}$ , the vector field  $\tilde{\mathbf{v}} = (\tilde{u}, \tilde{v})$  is to leading order given by the vector field  $\tilde{\mathbf{v}}_0 \equiv (\tilde{u}_0, \tilde{v}_0)$ , and (13) shows that the flux through vertical lines is constant and entirely described by the dominant term  $\tilde{u}_0$ . The vector field  $\tilde{\mathbf{v}}_0$  therefore gives an explicit description of the asymptotic flow downstream of the body as the sum of two divergence-free contributions: a parabolic wake term (multiplied by  $c$ ), and a compensating source term (multiplied by  $d$ ). Note that the asymptotic behavior  $\tilde{\mathbf{v}}_0$  is universal, in the sense that this asymptotic is independent of the geometry of the body, except for the amplitudes  $c$  and  $d$ . From (6), (7) we get in the original coordinates

$$u_0(x, y) = \left( v_\infty \sqrt{\ell} \right) \frac{c}{2\sqrt{\pi}} \frac{1}{\sqrt{x}} e^{-\frac{y^2}{4\ell x}} + (v_\infty \ell) \frac{d}{\pi} \frac{x}{x^2 + y^2} , \quad (14)$$

$$v_0(x, y) = \left( v_\infty \sqrt{\ell} \right) \frac{c}{4\sqrt{\pi}} \frac{y}{x^{3/2}} e^{-\frac{y^2}{4\ell x}} + (v_\infty \ell) \frac{d}{\pi} \frac{y}{x^2 + y^2} . \quad (15)$$

## 2.2 Adaptive boundary conditions

We now define the vector field  $\mathbf{v}_{ABC} = (u_{ABC}, v_{ABC})$  that we use on the boundary  $\Gamma$  (see Figure 1). Namely, for  $(x, y) \in \Omega$ ,  $x > 0$  (and therefore in particular on  $\Gamma_E$  and on  $\Gamma_N^+$  and  $\Gamma_S^+$ ) we set

$$u_{ABC}(x, y) = u_0(x, y) , \quad (16)$$

$$v_{ABC}(x, y) = v_0(x, y) , \quad (17)$$

with  $u_0$  and  $v_0$  as defined in (14), (15), while for  $(x, y) \in \Omega$ ,  $x \leq 0$  (and therefore in particular on  $\Gamma_W$  and on  $\Gamma_N^-$  and  $\Gamma_S^-$ ) we set

$$u_{ABC}(x, y) = (v_\infty \ell) \frac{d}{\pi} \frac{x}{x^2 + y^2}, \quad (18)$$

$$v_{ABC}(x, y) = (v_\infty \ell) \frac{d}{\pi} \frac{y}{x^2 + y^2}. \quad (19)$$

Furthermore we set

$$d = -\frac{c}{2}, \quad (20)$$

$$c = -\frac{1}{\rho \ell v_\infty^2} F, \quad (21)$$

where  $F$  is the total drag acting on the body.

This Ansatz is well motivated on  $\Gamma_E$  by (11), (12), and on those parts of the boundary  $\Gamma_N^+$  and  $\Gamma_S^+$  where  $x \gg 1$ . Note that, for large enough domains  $D$ , the contribution of the wake-term (term multiplied by  $c$ ) is on  $\Gamma_N^+$  and  $\Gamma_S^+$  negligible with respect to the source term (term multiplied by  $d$ ), so that asymptotically  $\mathbf{v}_{ABC}$  is given by (18), (19) on all of  $\Gamma \setminus \Gamma_E$ . This choice is well motivated (see [12]) by realizing that the source term is a gradient field with potential  $\psi(x, y) = \log(\sqrt{x^2 + y^2})$ , and that  $\psi$  is the real part of the function  $\varphi$ ,  $\varphi(x + iy) = \log(x + iy)$ , which extends to a holomorphic function in  $\Omega$ . Finally, the wake term on  $\Gamma_N^+$  and  $\Gamma_S^+$  interpolates smoothly between the asymptotic behavior for large values of  $x$  and the boundary conditions on  $\Gamma_N^-$  and  $\Gamma_S^-$ , and ensures moreover that the total flux through the boundary  $\Gamma$  is zero. Namely consider as in Figure 1, an arbitrary rectangle with boundary  $S$  containing the body  $\mathbf{B}$ . Since the total flux of a constant vector field  $\mathbf{v}|_{\partial \mathbf{B}} = -\mathbf{v}_\infty$  through  $\partial \mathbf{B}$  is zero and since the vector field  $\mathbf{v}$  is divergence free, it follows using Gauss's theorem that the total flux through  $S$  has to be zero as well. This is certainly true for Dirichlet boundary conditions. For the vector field  $\mathbf{v}_{ABC}$  we find from (20), and using in addition that  $\mathbf{v}_{ABC}$  is manifestly divergence free and smooth, that

$$\begin{aligned} & \int_S \mathbf{v}_{ABC} \cdot \mathbf{n} \, d\sigma \\ &= \lim_{L \rightarrow \infty} \left[ \int_{-L}^L (u_{ABC}(x_2, y) - u_{ABC}(x_1, y)) \, dy \right. \\ & \quad \left. + \int_{x_1}^{x_2} (v_{ABC}(x, L) - v_{ABC}(x, -L)) \, dx \right] \\ &= \lim_{L \rightarrow \infty} \int_{-L}^L (u_{ABC}(x_2, y) - u_{ABC}(x_1, y)) \, dy \\ &= (v_\infty \ell) (c + 2d) = 0. \end{aligned}$$

To relate  $c$  to the total drag  $F$  on the body we integrate the Navier-Stokes equation over  $S$  (see [7], [4]). Assuming that  $\mathbf{v} - \mathbf{v}_{ABC}$  satisfies a bound similar to (11), (12) not only in the wake region but everywhere on  $S$ , and that  $p \approx p_{ABC} = -\frac{1}{2}(u_{ABC}^2 + v_{ABC}^2)$ , asymptotically as  $S$  converges to infinity, we get that

$$\begin{aligned} F &= \lim_{L \rightarrow \infty} - \int_{-L}^L \left[ \left( p_{ABC}(x_2, y) - \rho [v_\infty + u_{ABC}(x_2, y)]^2 \right) \right. \\ & \quad \left. - \left( p_{ABC}(x_1, y) - \rho [v_\infty + u_{ABC}(x_1, y)]^2 \right) \right] \, dy \\ &= -\rho v_\infty^2 \ell \, 2(c + d) \\ &= -(\rho v_\infty^2 \ell) \, c, \end{aligned}$$

as claimed in (21). This completes the definition of the adaptive boundary conditions.

### 3 Solution process

For a domain  $\Omega \subset \mathbf{R}^2$ , let  $L^2(\Omega)$  denote the Lebesgue space of square-integrable functions on  $\Omega$  equipped with the inner product and norm

$$(f, g)_\Omega = \int_\Omega fg \, dx, \quad \|f\|_\Omega = (f, f)_\Omega^{1/2}.$$

The pressure is assumed to lie in the space  $L_0^2(\Omega) := \{q \in L^2(\Omega) : \int_\Omega q = 0\}$ , which defines it uniquely assuming  $\Omega' \subset \Omega$  bounded. The  $L^2(\Omega)$  functions with generalized (in the sense of distributions) first-order derivatives in  $L^2(\Omega)$  form the Sobolev space  $H^1(\Omega)$ , while  $H_0^1(\Omega) = \{v \in H^1(\Omega), v|_{\partial\Omega} = 0\}$ .

#### 3.1 Galerkin finite element discretization

The Galerkin finite element method starts from a variational formulation of the equations (3) to be solved. Let  $W = [H_{loc}^1(\Omega)]^2 \times L_0^2(\Omega)$ . For  $\mathbf{w} = \{\mathbf{v}, p\} \in W$  and  $\phi = \{\varphi, q\} \in W$ , we define the semi-linear form

$$\mathcal{A}(\mathbf{w}; \phi) = \rho(((\mathbf{v} + \mathbf{v}_\infty) \cdot \nabla) \mathbf{v}, \varphi)_\Omega - (p, \nabla \cdot \varphi)_\Omega + 2\mu \int_D \mathcal{D}(\mathbf{v}) : \mathcal{D}(\varphi) - (\nabla \cdot \mathbf{v}, q)_\Omega, \quad (22)$$

which is obtained by testing the equations (3) by  $\phi \in W$  and by partial integration of the diffusive term and the pressure gradient (see e.g. [20, 8, 9, 24, 15] for more details).  $\mathcal{D}(\mathbf{v})$  denotes the deformation tensor, i.e.,  $\mathcal{D}(\mathbf{v}) = \frac{1}{2}(\nabla \mathbf{v} + (\nabla \mathbf{v})^T)$ . A weak form of the equations (3) can be formulated as:

find  $\mathbf{w} = \{\mathbf{v}, p\} \in W$ , such that

$$\mathcal{A}(\mathbf{w}; \phi) = 0, \quad \forall \phi \in W. \quad (23)$$

In order to solve (23) numerically by a Galerkin finite element method, the unbounded domain  $\Omega$  is replaced by a bounded domain  $D \subset \Omega$ . The discretization uses a conforming finite element space  $W_h \subset W$  defined on quasiuniform triangulations  $\mathcal{T}_h = \{K\}$  consisting of quadrilateral or hexahedral cells  $K$  covering the domain  $D$ . For the trial and test spaces  $W_h \subset [H_0^1(D)]^2 \times L_0^2(D)$  we consider the standard Hood-Taylor finite element [16], i.e., we define

$$W_h = \{(v, p) \in [C(\overline{D})]^3; v|_K \in [Q_2]^2, p|_K \in Q_1\},$$

where  $Q_r$  describes the space of isoparametric tensor-product polynomials of degree  $r$  (for a detailed description of this standard construction process see for example [5]). This choice for the trial and test functions has the advantage that it guarantees a stable approximation of the pressure since the uniform *Babuska-Brezzi* inf-sup stability condition is satisfied uniformly in  $D$  (see [6] and references therein). The advantage, when compared to equal order function spaces for the pressure and the velocity is that no additional stabilization terms are needed. The discrete counterpart of problem (23) then reads:

find  $\mathbf{w}_h = \{\mathbf{v}_h, p_h\} \in \mathbf{w}_{b,h} + W_h$ , such that

$$\mathcal{A}(\mathbf{w}_h; \phi_h) = 0, \quad \forall \phi_h \in W_h. \quad (24)$$

Here  $\mathbf{w}_{b,h}$  describes the prescribed Dirichlet data on the boundary  $\Gamma$  of the domain  $D$ . A straightforward approach consists in considering a domain  $D$  which is large enough such that  $\mathbf{v} \approx 0$  in  $\Omega \setminus D$ . This leads to homogeneous Dirichlet boundary conditions for  $\mathbf{v}$  on  $\Gamma$ . As will be shown in Section 4, when computing quantities such as the drag or lift, this simplification is valid only for domains  $D$  which are typically several order of magnitude bigger than  $\mathbf{B}$ . In practice this leads to extremely large and untractable discrete problems. The goal of the adaptive boundary conditions proposed in Section 2 is to avoid this problem by imposing adequate non-homogeneous Dirichlet boundary conditions on  $\Gamma$ . These boundary conditions correspond to the asymptotics of  $\mathbf{v}$  in  $\Omega \setminus D$ . As has been discussed in Section 2, this asymptotics is independent of the details of the geometry of the body, but depends on the drag. The accurate computation of the drag is therefore an important issue.

#### 3.2 Computation of the drag

Let  $\sigma(\mathbf{v}, p) = -pI + 2\mu\mathcal{D}(\mathbf{v})$  denote the stress tensor. The force acting on the rigid body  $\mathbf{B}$  in the direction  $\psi$  on  $\partial\mathbf{B}$  is given by

$$N_\psi(\mathbf{w}) = \int_{\partial\mathbf{B}} (\sigma(\mathbf{v}, p) \cdot \mathbf{n}) \cdot \psi, \quad (25)$$

where  $\mathbf{w} = (\mathbf{v}, p)$ ,  $\psi \in [H^{1/2}(\partial\mathbf{B})]^2$  and where  $n$  is the unit outward normal to  $\partial\mathbf{B}$ . If  $\psi$  is a unit vector parallel (resp. perpendicular) to the flow direction, then  $N_\psi(\mathbf{w})$  is referred to as the drag (resp. lift). Let  $\tilde{\psi} \in H^1(D)$  be defined such that

$$\tilde{\psi} = \psi \quad \text{on } \partial\mathbf{B}, \quad \tilde{\psi} = 0 \quad \text{on } \Gamma. \quad (26)$$

Applying Green's identity to the integral (25) leads to the equality

$$N_\psi(\mathbf{w}) = \mathcal{A}(\mathbf{w}; \tilde{\psi}). \quad (27)$$

The expression (27) holds for any smooth  $\mathbf{w}$  and for any choice of  $\tilde{\psi}$  fulfilling the condition (26). We impose  $\tilde{\psi} \in W_h$ . Motivated by formula (27) we define the discrete counterpart  $N_\psi^h$  of  $N_\psi$  by the equation

$$N_\psi^h(\mathbf{w}_h) = \mathcal{A}(\mathbf{w}_h; \tilde{\psi}). \quad (28)$$

Again, under the assumptions (26), the right-hand side of (28) is independent of the choice of  $\tilde{\psi} \in W_h$  and  $N_\psi^h$  is therefore well defined. It is important to note that

$$N_\psi^h(\mathbf{w}_h) \neq N_\psi(\mathbf{w}_h).$$

Based on the Babuska-Miller trick [1, 2, 3], Giles et al. proved in [11] that  $N_\psi^h(\mathbf{w}_h)$  is indeed the adequate formulation for the computation of the drag. Assuming boundaries which are sufficiently smooth, they show that the order of convergence of  $N_\psi^h(\mathbf{w}_h)$  to  $N_\psi(\mathbf{w})$  is  $O(h^4)$  which is to be compared to an order of convergence of typically  $O(h^2)$  for the direct approximation of  $N_\psi$ . A typical example is shown in Table 1 which makes clear that the evaluation of the drag through the formulation (28) is essential in order to attain the accuracy needed here with reasonable computational cost.

Level	# Unknowns	drag computed by means of	
		$N_\psi^h(\mathbf{w}_h)$	$N_\psi(\mathbf{w}_h)$
3	18,592	-0.0504563	-0.0522906
4	74,048	-0.0503341	-0.0516217
5	295,552	-0.0503143	-0.0512033
6	1,180,928	-0.0503102	-0.0509204

Table 1: Convergence records of the drag considering both formulations  $N_\psi^h(\mathbf{w}_h)$  and  $N_\psi(\mathbf{w}_h)$ . We refer to Section 4 for the description of the considered configuration. The computational domain has a diameter that is eight hundred ( $d = 800$ ) times bigger than that of the rigid body.

### 3.3 Solver

In our approach, the nonlinear algebraic system (24) is solved implicitly in a fully coupled manner by means of a damped Newton method. Denoting the derivatives of  $\mathcal{A}(\cdot, \cdot)$  taken at a discrete function  $\mathbf{w}_h \in W_h$  by  $\mathcal{A}'(\mathbf{w}_h, \cdot)(\cdot)$ , the linear system arising at the Newton step number  $k$  has the following form,

$$\mathcal{A}'(\mathbf{w}_h^k, \phi_h)(\tilde{\mathbf{w}}_h^k) = (\mathbf{r}_h^k, \phi_h), \quad \forall \phi_h \in W_h, \quad (29)$$

where  $\mathbf{r}_h^k$  is the equation residual of the preceding approximation  $\mathbf{w}_h^k$ , and where  $\tilde{\mathbf{w}}_h^k$  corresponds to the needed correction. The updates  $\mathbf{w}_h^{k+1} = \mathbf{w}_h^k + \alpha^k \tilde{\mathbf{w}}_h^k$  with a relaxation parameter  $\alpha^k$  chosen by means of Armijo's rule are carried out until convergence. In practice, the Jacobian involved in (29) is directly derived from the analytical expression for the derivative of the variational system (24).

It is well known that the ability to converge at the local rate of the Newton iteration greatly depends on the quality of the initial approximation (see e.g. [17]). In order to find such an initial approximation, we consider a mesh hierarchy  $\mathcal{T}_{h_i}$  with  $\mathcal{T}_{h_i} \subset \mathcal{T}_{h_{i+1}}$ , and the corresponding system of equations (24) is successively solved by taking advantage of the previously computed solution, i.e., the nonlinear Newton steps are embedded in a *nested iteration* process (see e.g. chapter 8, [26]).

The linear subproblems (29) are solved by the *Generalized Minimal Residual Method (GMRES)* (see Saad [21]) preconditioned by means of multigrid iteration (see [27, 26] and references therein for the description of the different multigrid techniques for flow simulations). This preconditioner, based on a new multigrid scheme oriented towards conformal higher order FEM, is a key ingredient of the overall solution process. Two specific features characterize the proposed scheme: varying orders of the FEM ansatz on the mesh hierarchy and a Vanka-type smoother [25] adapted to higher order discretization. This somewhat technical part of the solver is described in full details in [14]. Its implementation is part of the HiFlow project (see [13]).

The specificity of our approach is to prescribe boundary conditions which depend on the drag. The drag, and therefore the adequate boundary conditions, are clearly not known at the beginning of the resolution process. In order to cope with this problem the Newton steps previously described are embedded in an additional fixed point iteration which determines the drag through successive updates of the boundary conditions based on the previously computed drag.

## 4 Numerical experiments

The goal of this section is twofold. On one hand we compare, for a given configuration of the flow, the solution obtained by means of the newly proposed boundary conditions (see Section 2) with the solution obtained by means of homogeneous Dirichlet boundary conditions. This first step confirms the theoretical results developed in [28, 29] and gives numerical evidence on the validity of our approach towards a correct modelisation and numerical simulation of exterior flow problems. On the other hand, quantitative results depicted for different Reynolds numbers clearly show the generally drastic improvements in numerical efficiency when considering the proposed boundary conditions.

Our model problem consists of a rectangle  $[-0.1, 0.1] \times [-0.5, 0.5]$  which is immersed into a uniform stream of a homogeneous incompressible fluid with density  $\rho = 1$  and dynamic viscosity  $\mu = 0.1$ . Further we impose  $u_\infty = 0.1$ . With  $A = 1$  being the length of the rectangle, we find from (4) for the Reynolds number corresponding to this configuration,

$$Re = \frac{A \rho v_\infty}{\mu} = 1. \quad (30)$$

For the computational domain  $D$  we restrict ourselves to square domains. Due to limitations inherent to the solver, the aspect ratio of the considered meshes does not exceed  $\tau = 30$ . Typical meshes corresponding to this setup are depicted in Figure 3.

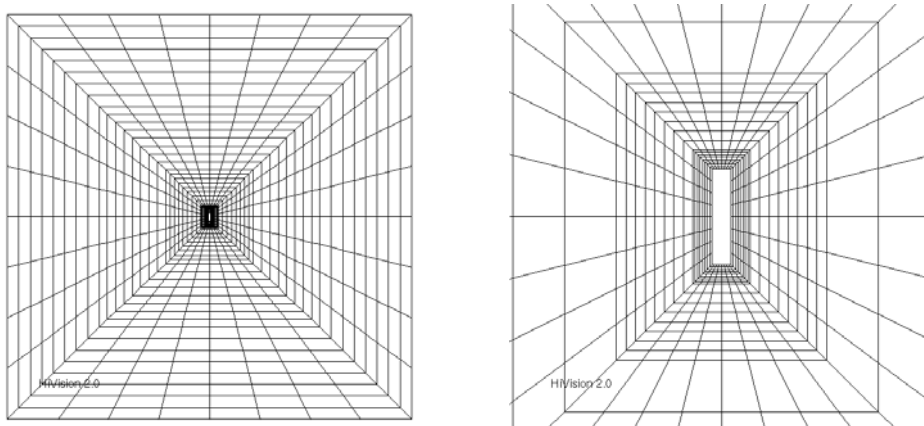


Figure 3: On the left, third refinement grid considered for the triangulation of the computational domain  $D$ . The diameter of  $D$  is equal to  $d = 50$ . On the right, zoom of the mesh around the rigid body  $\mathbf{B}$ .



## 4.1 Validation of the boundary conditions

We now discuss various ways of comparing the numerical solutions  $\mathbf{v} = (u, v)$  of (3) (obtained with Dirichlet and adaptive boundary conditions) with the theoretical predictions. We start by considering the wake region, where we have the most precise results (see [29]). A quantity which has been intensively studied (see for example [23] and [22]) is the so called centerline velocity  $\mathbf{v}(x, 0)$  (see Figure 1 for the definition of cut I, cut II, and cut III). Since  $u$  is even and  $v$  is odd in  $y$  we have that  $v(x, 0) = 0$  for all  $x$ , and we therefore only need to consider  $u(x, 0)$ . The theoretical prediction (14), (21), (20) is that, to leading order for large  $x$ ,

$$u(x, 0) \approx \left( v_\infty \sqrt{\ell} \right) \frac{c}{2\sqrt{\pi}} \frac{1}{\sqrt{x}}, \quad (31)$$

with

$$c = -\frac{1}{\rho \ell v_\infty^2} F. \quad (32)$$

In Figure 6 we have plotted the quantity  $-2\sqrt{\pi}\sqrt{x}u(x, 0)$  as a function of  $x$ , where  $u$  has been computed once using Dirichlet boundary conditions and once using the adaptive scheme. Numerically we find that  $F = -0.05031$ . We therefore expect using (31) that  $-2\sqrt{\pi}\sqrt{x}u(x, 0) \approx -\left( v_\infty \sqrt{\ell} \right) c = 0.5031$  for large values of  $x$ . As Figure 6 shows, the solution with Dirichlet boundary conditions indeed appears to converge to this value, but most of the computational domain is lost for the interpolation between this correct asymptotic value and the value zero imposed by the boundary conditions. With the adaptive boundary conditions (see Figure 6 right) only minor (higher order) corrections are necessary when arriving to the boundary, the plot being close to the asymptotic value on most of the domain.

On cut II, perpendicular to the body, both components of  $\mathbf{v}$  are non zero, but the  $v$ -component is asymptotically dominant. The theory (19), (20), (21) predicts that, asymptotically, for large values of  $y$ ,

$$v(0, y) \approx -\left( v_\infty \ell \right) \frac{c}{2\pi} \frac{1}{y}, \quad (33)$$

with  $c$  again given by (32). In Figure 7 we have plotted the quantity  $2\pi y v(0, y)$  as a function of  $y$ , and  $v$  has been computed using Dirichlet boundary conditions and using the adaptive scheme. From (33) we expect that  $2\pi y v(0, y) \approx -\left( v_\infty \ell \right) c = 0.5031$  for large values of  $y$ . Indeed, for values of  $y$  that are large compared to the size of  $\mathbf{B}$ , but small compared to the size of the computational domain (i.e.,  $y \approx 100$ ) the graphs in Figure 7 appear to level off at a value compatible with the theoretical prediction, but then rapidly go to zero, in a domain dependent way, as required by the Dirichlet boundary conditions. In the adaptive scheme the asymptotic value is enforced at the boundary, and we get, with increasing computational domains, a sequence of graphs that appear to converge to some limiting graph that is consistent with the asymptotic prediction (33).

On cut III, finally, the  $v$ -component is again zero and for  $u$  we have the prediction that, asymptotically, for very negative values of  $x$ ,

$$u(x, 0) \approx -\left( v_\infty \ell \right) \frac{c}{2\pi} \frac{1}{x}, \quad (34)$$

with  $c$  as above. In Figure 8 we have plotted the quantity  $2\pi x u(x, 0)$  as a function of  $x$ . For this cut the results are even more drastic. For the adaptive boundary conditions we get a sequence of graphs that converge quite clearly to some limiting graph which is moreover compatible with the asymptotic prediction (34). The sequence of graphs for Dirichlet boundary conditions does not converge at all for this case, but depends on the whole range of volumes very strongly on the boundary condition.

We conclude that, as expected, physically interesting quantities (in particular the drag) can a priori be computed using Dirichlet boundary conditions, but only by choosing the computational domain ridiculously large in order to leave “sufficient room” to accommodate for the non-physical backflow. The computation times are accordingly exceedingly large, so that some of these computations are in practice unfeasible.

This issue which is essential for the numerical simulation is depicted, quantitatively, in Figure 10. On this plot the relative error of the drag, as a function of the domain diameter is plotted considering the homogeneous Dirichlet boundary conditions and the proposed adaptive boundary conditions for  $\mu = 0.1$  ( $Re = 1$ ),  $\mu = 1$  ( $Re = 0.1$ ) and  $\mu = 10$  ( $Re = 0.01$ ). For  $\mu = 0.1$  ( $Re = 1$ ), a relative error of the drag equal to  $5 \cdot 10^{-2}$  can be obtained for the adaptive boundary conditions on a domain of diameter equal

to  $d_{ABC} = 80$  which is to be compared to a domain diameter equal to  $d_{Dir} = 800$  for the homogeneous Dirichlet case. For  $\mu = 1$  ( $Re = 0.1$ ), the same relative error can be attained for  $d_{ABC} = 300$  which is to be compared to  $d_{Dir} = 4000$ . For  $\mu = 10$  ( $Re = 0.01$ ), the discrepancy is even bigger since the relative error obtained for  $d_{ABC} = 600$  could not be obtained on domains with diameter less than 8000 for the homogeneous Dirichlet case. These results clearly illustrate the considerable increase of numerical efficiency associated with the proposed adaptive scheme.

## 4.2 Further results

Having established in Section 4.1 the validity of the adaptive scheme, we now present some additional results that illustrate in some more detail the basic ideas. All the numerical results for this section have been established with our standard configuration and  $\mu = 0.1$  ( $Re = 1$ ).

First, in Figure 4 the streamlines of the vector field  $\mathbf{u} = \mathbf{v}_\infty + \mathbf{v}$ , (the numerical solution of (1)) are shown. In contrast to streamlines computed with homogeneous Dirichlet boundary conditions, which are forced to be perpendicular to the wall when entering and leaving the domain, no such nonphysical deformations occur with the adaptive scheme. The same is true for the pressure isobars (see Figure 4).

We next discuss Figure 5 which shows the vorticity  $\omega$ ,  $\omega(x, y) = -\partial_y u(x, y) + \partial_x v(x, y)$ . The lines of constant vorticity join the right boundary perfectly natural. No deformation can be observed near the border. One also clearly sees that the vorticity is basically zero outside a rather small region around the object and outside the wake. In Figure 9 we have plotted the vorticity on vertical lines just before, after and somewhat more downstream of the object. As can be clearly seen the vorticity decays extremely rapidly in the directions transverse to the flow. The Fourier transform

$$\hat{\omega}(x, k) = \int_{\mathbf{R}} e^{iky} \omega(x, y) dy$$

is therefore a smooth function of  $k$  at  $k = 0$ , and this is the reason for the appearance of a parabolic wake (see [28]). This illustrates quite nicely the theorems and arguments of Section 2.

## 5 Conclusions and outlook

We have discussed the problem of solving numerically the stationary incompressible Navier-Stokes equations in a domain exterior to a body in two dimensions. A novel self-consistent scheme for choosing artificial boundary conditions has been introduced, which incorporates in particular the computation of the total drag exerted on a body as part of the solution process. When compared with the results obtained using traditional constant boundary conditions computational times are typically reduced by several orders of magnitude.

The present paper only discusses the case of symmetric bodies aligned with the fluid flow. Our method is however not intrinsically limited to this case: the generalization to the two-dimensional non-symmetric case and to the three-dimensional case will be treated in forthcoming publications.

### ACKNOWLEDGEMENT

Peter Wittwer is indebted to Prof. Rolf Rannacher for his immediate and positive response to the request for collaboration and for a kind invitation to Heidelberg which got this work started. Without his active and enthusiastic support this project would not have been possible. Peter Wittwer would also like to thank Prof. P. Monkewitz for several discussions and for very valuable pointers to the older literature. Vincent Heuveline would like to thank the department of Theoretical Physics for an invitation to Geneva. Sebastian Bönisch and Vincent Heuveline thank Prof. Rolf Rannacher for many fruitful discussions.

## References

- [1] I. Babuška and A. Miller. The post processing approach in the finite element method, part 1: calculation of displacements, stresses and other higher derivatives of the displacements. *Internat. J. Numer. Methods. Engrg.*, 34:1085–1109, 1984.

- [2] I. Babuška and A. Miller. The post processing approach in the finite element method, part 2: the calculation of stress intensity factors. *Internat. J. Numer. Methods. Engrg.*, 34:1111–1129, 1984.
- [3] I. Babuška and A. Miller. The post processing approach in the finite element method, part 3: a posteriori estimates and adaptive mesh selection. *Internat. J. Numer. Methods. Engrg.*, 34:1131–1151, 1984.
- [4] G. K. Batchelor. *A Introduction to Fluid Dynamics*. Cambridge University Press, 1967.
- [5] S.C. Brenner and R.L. Scott. *The mathematical theory of finite element methods*. Springer, Berlin-Heidelberg-New York, 1994.
- [6] F. Brezzi and R. Falk. Stability of higher-order Hood-Taylor methods. *SIAM J. Numer. Anal.*, 28(3):581–590, 1991.
- [7] A. Chorin and J. E. Marsden. *A Mathematical Introduction to Fluid Mechanics*. Interscience Publishers, Ltd., London, 1992.
- [8] G.P. Galdi. *An introduction to the mathematical theory of the Navier-Stokes equations: Linearized steady problems*. Springer Tracts in Natural Philosophy, Vol. 38, Springer-Verlag, 1998.
- [9] G.P. Galdi. *An introduction to the mathematical theory of the Navier-Stokes equations: Nonlinear steady problems*. Springer Tracts in Natural Philosophy, Vol. 39, Springer-Verlag, 1998.
- [10] G.P. Galdi. On the existence of symmetric steady-state solutions to the plane exterior navier-stokes problem for a large reynolds number. *Advances in Fluid Dynamics, Quaderni Di Matematica della II Universita' di Napoli*, 4:1–25, 1999.
- [11] M. Giles, M. Larson, M. Levenstam, and E. Süli. Adaptive error control for finite element approximations of the lift and drag coefficients in viscous flow. Technical Report NA-97/06, Oxford University Computing Laboratory, 1997.
- [12] S. Goldstein. *Lectures on Fluid Mechanics*. Interscience Publishers, Ltd., London, 1957.
- [13] V. Heuveline. **HiFlow** a general finite element C++ package for 2D/3D flow simulation. [www.hiflow.de](http://www.hiflow.de), 2000.
- [14] V. Heuveline. On higher-order mixed FEM for low Mach number flows: Application to a natural convection benchmark problem. *Int. J. Numer. Math. Fluids*, to appear.
- [15] J. G. Heywood, R. Rannacher, and S. Turek. Artificial boundaries and flux and pressure conditions for the incompressible navier-stokes equations. *Int. J. Numer. Math. Fluids*, 22:325–352, 1992.
- [16] P. Hood and C. Taylor. A numerical solution of the navier-stokes equations using the finite element techniques. *Comp. and Fluids*, 1:73–100, 1973.
- [17] C.T. Kelley. *Iterative methods for linear and nonlinear equations*, volume 16 of *Frontiers in Applied Mathematics*. SIAM, Philadelphia, 1995.
- [18] J. Leray. Sur le mouvement d'un liquide visqueux enlissant l'espace. *Acta Math.*, 63:1–25, 1934.
- [19] S. A. Nazarov and M. Specovius-Neugebauer. Nonlinear artificial boundary conditions with pointwise error estimates for the exterior three dimensional navier-stokes problem. *Math. Nachr.*, to appear, 2003.
- [20] R. Rannacher. Finite element methods for the incompressible Navier-Stokes equations. In Galdi Giovanni et al., editor, *Fundamental Directions in Mathematical Fluid Mechanics*, Advances in Mathematical Fluid Mechanics. Birkhäuser, 2000.
- [21] Y. Saad. *Iterative methods for sparse linear systems*. Computer Science/Numerical Methods. PWS Publishing Company, 1996.
- [22] I. J. Sobey. *Introduction to Interactive Boundary Layer Theory*. Oxford University Press, 2000.
- [23] K. Stewartson. On asymptotic expansions in the theory of boundary layers. *J. Maths Physics*, 36:173–191, 1957.
- [24] S. Turek. *Efficient solvers for incompressible flow problems. An algorithmic and computational approach*. Lecture notes in Computational Science and Engineering. Springer, 1999.
- [25] S. Vanka. Block-implicit multigrid calculation of two-dimensional recirculating flows. *Comp. Meth. Appl. Mech. Eng.*, 59(1):29–48, 1986.
- [26] P. Wesseling. *An introduction to multigrid methods*. Wiley, Chichester, 1992.
- [27] P. Wesseling and C.W. Oosterlee. Geometric multigrid with applications to computational fluid dynamics. *J. Comp. Appl. Math.*, 128:311–334, 2001.
- [28] P. Wittwer. On the structure of stationary solutions of the navier-stokes equations. *Commun. Math. Phys.*, 226:455–474, 2002.
- [29] P. Wittwer. Supplement: On the structure of stationary solutions of the navier-stokes equations. *Commun. Math. Phys.*, to appear, 2003.

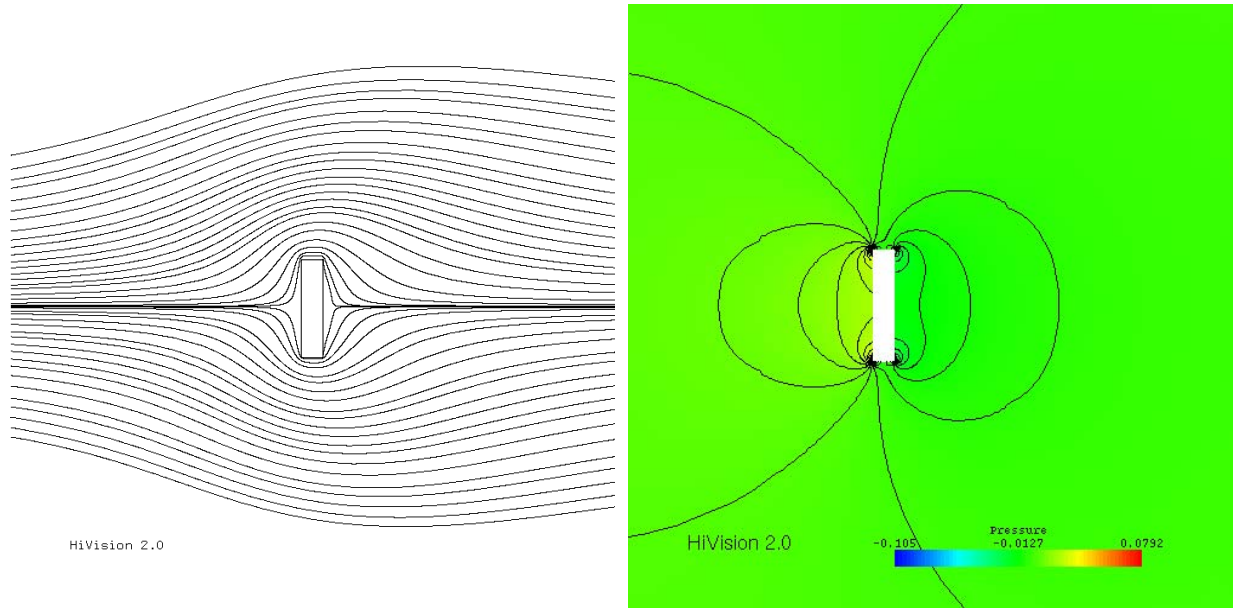


Figure 4: Streamlines (left) and pressure (right) around the body for the configuration described in Section 4.

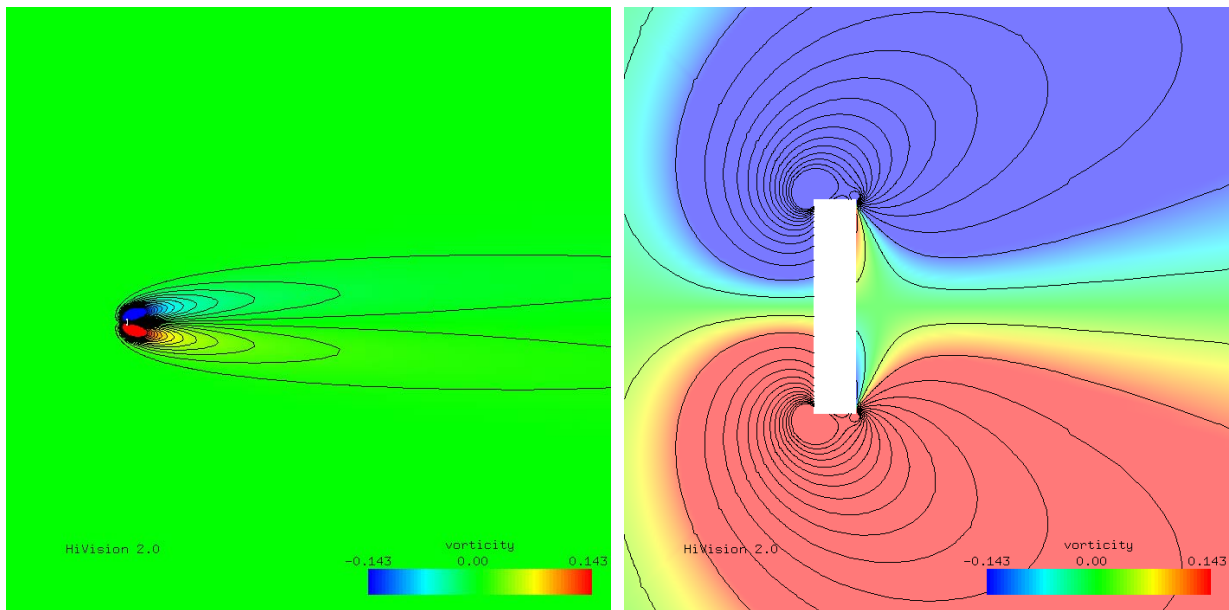


Figure 5: (left) Vorticity, (right) zoom on the vorticity for for the configuration described in Section 4

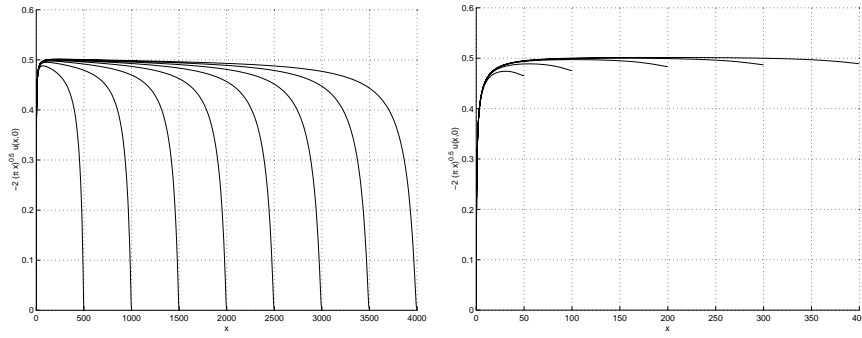


Figure 6: Scaled  $u$  component along cut I, considering homogeneous Dirichlet boundary conditions (left) and the proposed adaptive boundary conditions (right). For the homogeneous Dirichlet (resp. adaptive) boundary conditions the size of the diameter of the computational domain  $D$  varies in the range  $d \in [500; 4000]$  (resp.  $d \in [50; 400]$ ). Cut I, which is defined in Figure 1, reveals the asymptotics in the wake.

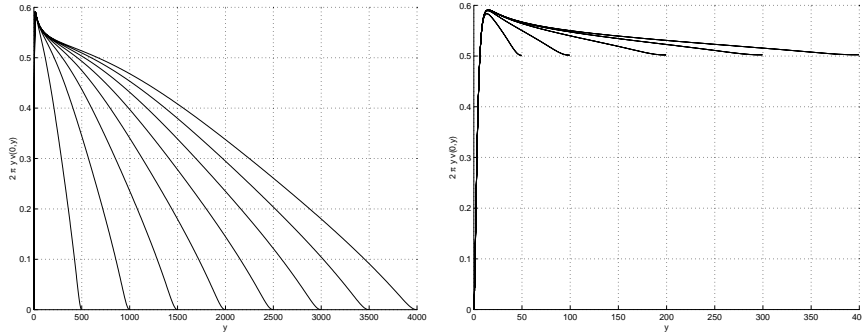


Figure 7: Scaled  $v$  component along cut II considering homogeneous Dirichlet boundary conditions (left) and the proposed adaptive boundary conditions (right). For the homogeneous Dirichlet (resp. adaptive) boundary conditions the size of the diameter of the computational domain  $D$  varies in the range  $d \in [500; 4000]$  (resp.  $d \in [50; 400]$ ). Cut II is defined in Figure 1.

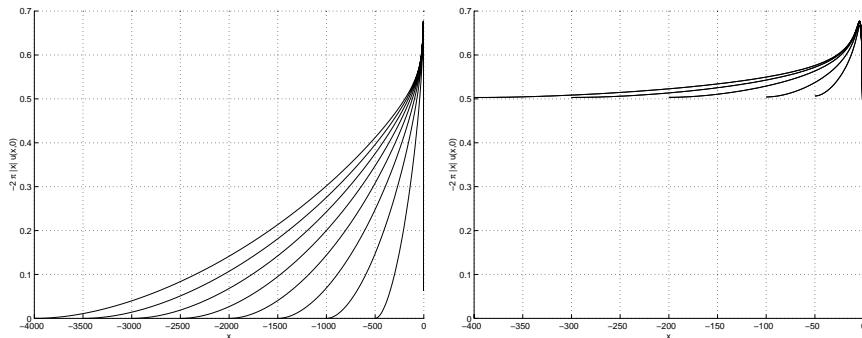


Figure 8: Scaled  $u$  component along cut III, considering homogeneous Dirichlet boundary conditions (left) and the proposed adaptive boundary conditions (right). For the homogeneous Dirichlet (resp. adaptive) boundary conditions the size of the diameter of the computational domain  $D$  varies in the range  $d \in [500; 4000]$  (resp.  $d \in [50; 400]$ ). Cut III is defined in Figure 1.

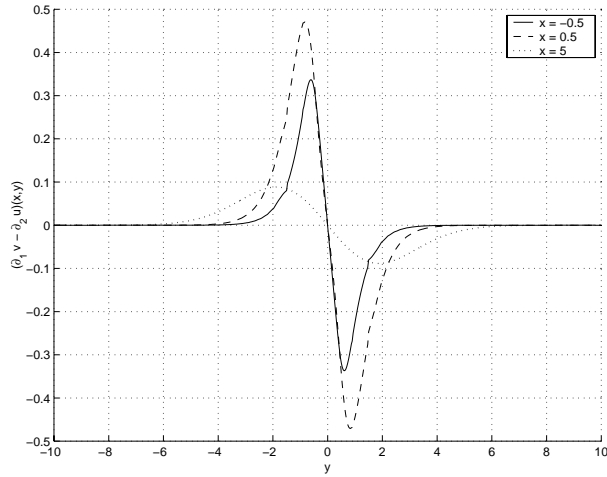


Figure 9: Vorticity on vertical lines for  $x = -2.5$ ,  $x = 2.5$  and  $x = 5$ .

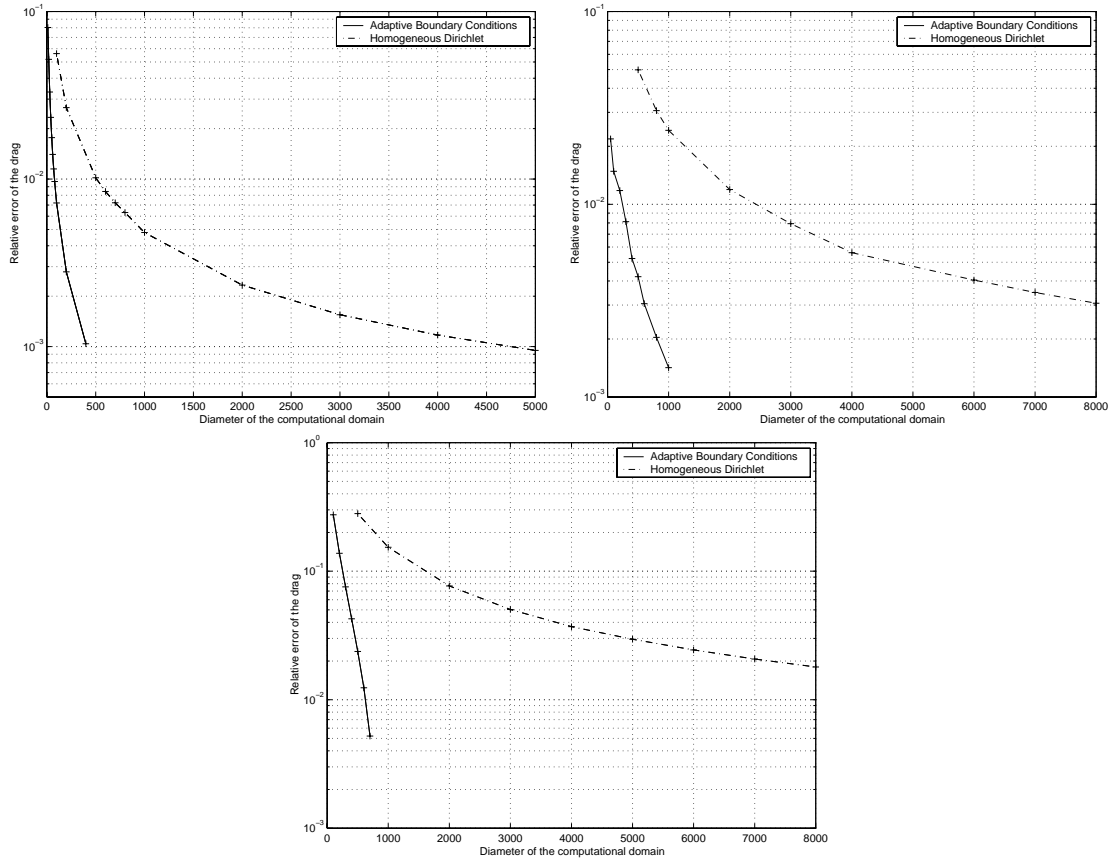


Figure 10: Plot of the relative error of the drag as a function of the domain diameter, considering homogeneous Dirichlet boundary conditions and the proposed adaptive boundary conditions, respectively. From left to right and top to bottom the plotted configurations correspond to  $\mu = 0.1$  ( $Re = 1$ ),  $\mu = 1$  ( $Re = 0.1$ ) and  $\mu = 10$  ( $Re = 0.01$ ).